Green/Yellow-Emitting Conjugated Heterocyclic Fluorophores for Luminescent Solar Concentrators

Papucci, Costanza; Geervliet, Tristan A.; Franchi, Daniele; Bettucci, Ottavia; Mordini, Alessandro; Reginato, Gianna; Picchioni, Francesco; Pucci, Andrea; Calamante, Massimo; Zani, Lorenzo

Published in:
European Journal of Organic Chemistry

DOI:
10.1002/ejoc.201800242

Publication date:
2018

ChemPubSoc Europe

DOI: 10.1002/ejoc.201800242

EurJOC European Journal of Organic Chemistry

Full Paper

Organic Fluorophores

SPECIAL ISSUE

Green/Yellow-Emitting Conjugated Heterocyclic Fluorophores for Luminescent Solar Concentrators

Costanza Papucci,[a,b,c] Tristan A. Geervliet,[d] Daniele Franchi,[a,c] Ottavia Bettucci,[a,b,c] Alessandro Mordini,[a,c] Gianna Reginato,[a] Francesco Picchioni,[d] Andrea Pucci,[e] Massimo Calamante*[a,c] and Lorenzo Zani*[a]

Abstract: In this study, we report on the synthesis of new organic fluorophores containing either the benzo[1,2-*d*:4,5-*d'*]bisthiazole or the dithieno[3,2-*b*:2',3'-*d*]silole heterocyclic unit, and on their application for the fabrication of luminescent solar concentrators (LSCs) made of poly(methyl methacrylate) (PMMA) thin films. In solution, the new compounds absorbed light in the visible region and displayed a brilliant green emission in the 500–600 nm range with moderate-to-good fluorescence quantum yields (0.25–0.68). Dispersions of selected fluorophores in PMMA thin films mostly maintained the light absorption features observed in solution, although in the case of benzobisthiazole-based fluorophore **1a** an evident fluorescence red-shift was observed when increasing the compound concentration in the film. In agreement with its promising optical properties, LSCs prepared with the latter compound yielded interesting optical efficiencies up to 6.42 %, not far from those of state-of-the-art PMMA LSC devices.

Introduction

Direct conversion of sunlight into electricity (photovoltaics) is widely regarded as a promising approach to ease the World's dependence on energy production by fossil fuels.[1] Despite the current steady growth of new photovoltaic (PV) installations,[2] full exploitation of this technology will be inevitably linked to a further reduction of solar power costs.[3] In this context, sunlight concentration appears a promising solution to yield cost-effective photovoltaic systems.[4]

Solar concentration works by harvesting incident sunlight on a large surface and redirecting it on a smaller area, thus allowing to reduce the amount of photoactive materials employed and, in turn, the final cost of the PV device. Compared to classical, geometrical concentrators, luminescent solar concentrators (LSCs) present several advantages, such as low cost and weight, transparency, high theoretical concentration factors and the ability to work with diffuse light without the need for tracking or cooling equipment.[5,6] Such features make LSCs especially well-suited for integration in modern building architectures, making ample use of colored windows and panels.[7] A typical LSC consists of a slab of transparent material (glass or polymer) doped with fluorescent dyes capable of absorbing light in a wide range of the solar spectrum.[6,7] Due to the higher refractive index of the host material compared to the environment, a large fraction of light re-emitted by the fluorophores is trapped by total internal reflection, and is collected at the edges of the device where photovoltaic modules can be placed to produce electric power.

Despite their advantages, LSCs are still affected by significant drawbacks limiting their photovoltaic performances, often due to light re-absorption and fluorescence quenching upon dye aggregation.[8] For this reason, research on LSC materials has focused on the development of new fluorescent emitters characterized by a series of ideal properties, such as broad absorption range, high fluorescence quantum yield, limited (or no) overlap between absorption and emission spectra (i.e. large Stokes shift) and good solubility in the host matrix.[9] Obviously, satisfying all these criteria is not an easy task. For example, red-emitting organic fluorophores are usually preferred since their emission wavelengths match well with the band-gap of Si-based PV modules,[10,11] but they tend to strongly quench their own fluorescence in condensed phases, thus seriously limiting the generation of electric current.[12]

Various different materials have been considered as fluorescent emitters for LSCs, such as colloidal quantum dots, metal-organic complexes and organic dyes.[9,13] Among the latter, perylene-based compounds have received special attention, thanks to the high efficiencies of the corresponding devices.[14–18] In

[a] *Institute of Chemistry of Organometallic Compounds (CNR-ICCOM), Via Madonna del Piano 10, 50019 Sesto Fiorentino, Italy*
E-mail: m.calamante@iccom.cnr.it
lorenzo.zani@iccom.cnr.it
www.iccom.cnr.it
[b] *Department of Biotechnology, Chemistry and Pharmacy, University of Siena, Via A. Moro 2, 53100 Siena, Italy*
[c] *Department of Chemistry "U. Schiff", University of Florence, Via della Lastruccia 13, 50019 Sesto Fiorentino, Italy*
[d] *Department of Chemical Engineering, University of Groningen, Nijenborgh 4, 9747 AG Groningen, The Netherlands*
[e] *Department of Chemistry and Industrial Chemistry, University of Pisa, Via A. G. Moruzzi 13, 56124 Pisa, Italy*
Supporting information and ORCID(s) from the author(s) for this article are available on the WWW under https://doi.org/10.1002/ejoc.201800242.

particular, Lumogen F Red 305 (LR, Figure 1) is currently considered the state-of-the-art for LSCs due to its very high fluorescence quantum yield and its excellent photostability.[13,19] Despite that, its very small Stokes shift could still limit its actual use for the large-scale deployment of LSC technology. Besides perylene derivatives, only few examples of LSCs doped with organic fluorophores were recently reported in the literature, including dicyanomethylene laser dyes,[20] benzothiazoles,[21] benzothiadiazoles,[22] diketopyrrolopyrroles,[23] an AIEgen dye,[24] a silafluorene,[25] fluorene-BODIPY oligomers[26] and a silicon-containing phthalocyanine.[27]

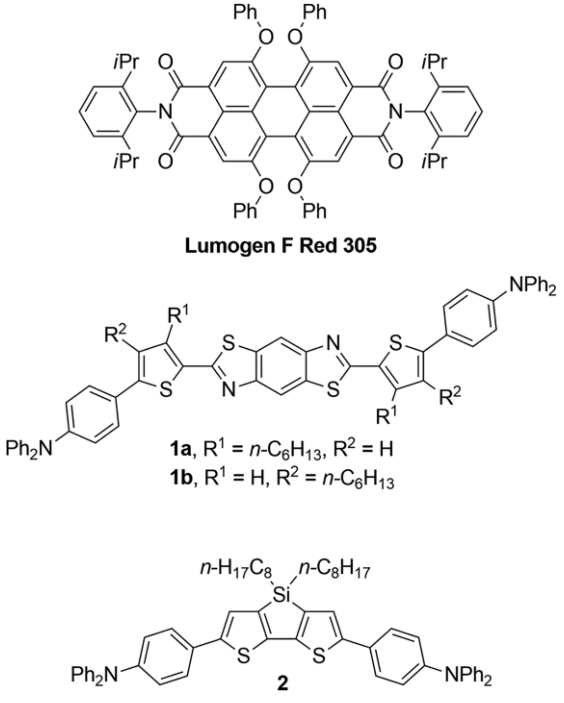

Figure 1. Structures of Lumogen F Red 305 and of fluorophores **1a**,**b** and **2**.

Due to the self-quenching problems often encountered with red fluorescent dyes, we focused our attention on green-emitting compounds, aiming to optimize their optical properties towards application as fluorophores in LSCs. In particular, during our studies on the synthesis of organic sensitizers for dye-sensitized solar cells,[28] we observed that intermediates containing the benzo[1,2-*d*:4,5-*d'*]bisthiazole (BBT) heterocyclic core displayed intense green fluorescence upon visible light irradiation. Indeed, a literature survey showed that substituted BBT derivatives can show broad emission from decay of charge-transfer states[29] and were used as emitters in LED devices[30] and as fluorescent probes in biomedical imaging.[31] Based on these data, we reasoned that BBT derivatives could also be used as fluorescent emitters for LSCs, and designed compounds **1a** and **1b** (Figure 1). The central electron withdrawing BBT unit was decorated with electron donating triphenylamine groups connected via thiophene rings, with the aim to strengthen and red-shift both absorption and emission spectra thanks to intramolecular charge transfer. Alkyl chains were placed on the thiophene rings in different positions in order to increase the solubility of the resulting compounds and to determine how their different conformations could influence their photophysical properties.

In addition, we also wanted to compare the photovoltaic results provided by BBT derivatives with those of a reference compound having similar optical properties (at least in solution), but bearing a different heterocyclic unit, in order to determine how the change of the central core would influence the overall device performance. To this end, we selected dithieno[3,2-*b*:2′,3′-*d*]silole (DTS), due to the fact that DTS-based compounds had found extensive use in organic electronics and photovoltaics,[32,33] and had been previously applied as blue-green photo- and electroluminescent materials[34] as well as fluorescent chemosensors.[35] For application in LSCs, we designed compound **2** (Figure 1), in which the DTS core was flanked by the same triphenylamine end groups of fluorophores **1a** and **1b**.

Herein, we report the synthesis and the spectroscopic characterization of compounds **1a**, **1b** and **2** both in solution and embedded in PMMA films. In addition, we describe the photovoltaic performances of thin-film LSC devices prepared with the new dyes. The thin film configuration was chosen since it allows an easy and fast set-up, which are the conditions required for rapid parameters optimization of LSC samples. The light concentration and optical efficiencies of the derived LSCs were determined with a properly designed set-up.

Results and Discussion

Synthesis of Fluorophores 1a, 1b, and 2

In our design, we sought to extend the conjugation of the central heterocyclic BBT and DTS moieties by introduction of additional thiophene rings and triphenylamine units. Nevertheless, structures of compounds **1a** and **1b** and **2** were kept simple and easy to prepare, bearing in mind that the main justification for the LSC approach is cost reduction compared to traditional PV. The procedure followed to prepare compounds **1a** and **1b** is shown in Scheme 1, while that used to obtain compound **2** is presented in Scheme 2.

Starting with the synthesis of BBT derivatives, commercially available bromides **3a** and **3b** were converted into the corresponding aldehydes by adapting a known synthetic procedure.[36] Formation of the BBT tricyclic core was then accomplished by reaction of the aldehydes with 2,5-diaminobenzene-1,4 dithiol bis-hydrochloride (**5**), similar to our previously reported procedure:[28] in this case, however, it was found that by working in anhydrous toluene rather than *N*,*N*-DMF the reaction proceeded much more cleanly, simplifying product purification (at the expense of a slightly lower conversion, which led to essentially the same isolated yield). After bromination of intermediates **6a** and **6b**, the resulting dibromo derivatives **7a** and **7b** were finally subjected to Suzuki–Miyaura cross-coupling with boronic acid **8** to give the desired target compounds **1a** and **1b**. It was found that use of [Pd(dppf)Cl_2] as the catalyst in combination with KF as the base gave a better yield of the final

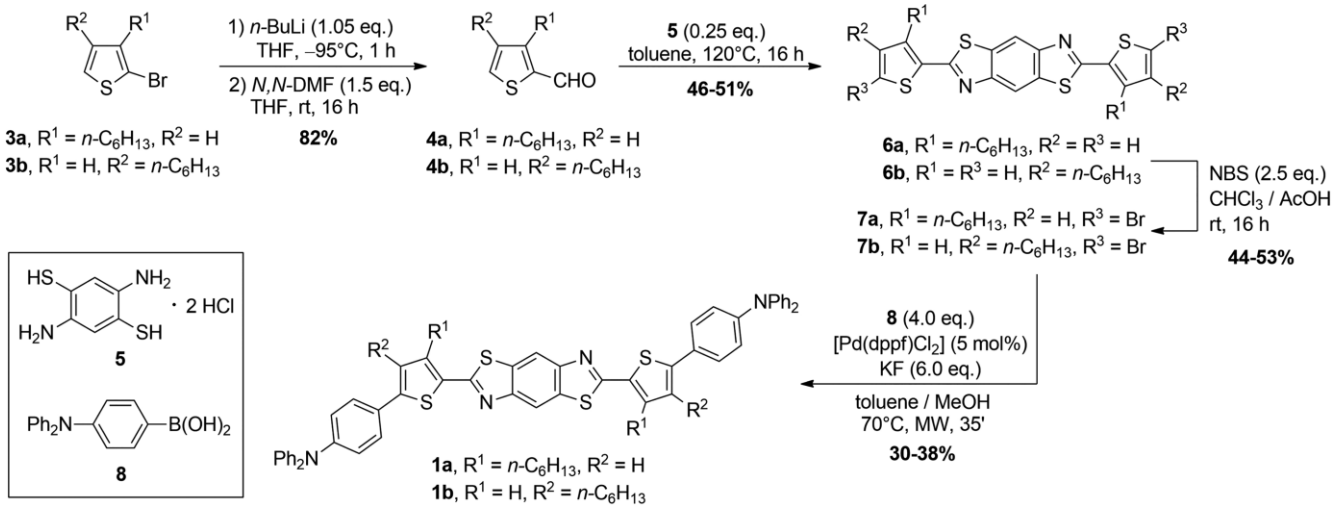

Scheme 1. Synthesis of compounds **1a** and **1b**.

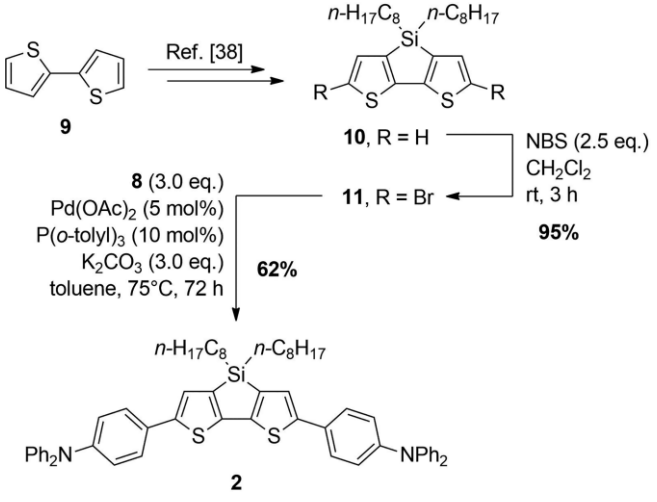

Scheme 2. Synthesis of compound **2**.

products,[37] and employment of microwave irradiation allowed to significantly shorten reaction times (approx. 35 min. compared to several hours under convection heating).

Concerning compound **2**, the synthesis started with bisthiophene (**9**), which was converted to 4,4′-bis-(*n*-octyl)-dithieno-[3,2-*b*:2′,3′-*d*]silole (**10**) by means of a known synthetic procedure.[38] The latter compound was subjected to electrophilic bromination to give derivative **11**, which was finally converted into the desired product through a Suzuki–Miyaura coupling with boronic acid **8**. Importantly, in this case the best result was obtained when using the more basic tris-(*o*-tolyl)phosphine instead of PPh_3 as a ligand for palladium, which allowed to speed oxidative addition up at the beginning of the catalytic cycle and efficiently minimized protodesilylation of the starting material.

Spectroscopic Characterization in Solution

The optical properties of compounds **1a**,**b** and **2** were investigated by means of UV/Vis absorption spectroscopy and fluorescence emission spectroscopy in solution. The solvent chosen was ethanol since it efficiently dissolved the compounds while having a refractive index (1.37) similar to that of PMMA (1.50). The relevant data are presented in Table 1 and the spectra are shown in Figure 2.

Table 1. Spectroscopic properties of compounds **1a**, **1b**, and **2**.

Cmpd.	λ_{abs} [nm]	ε [M^{-1} cm^{-1}]	λ_{emi} [nm]	SS [nm][a]	Φ_f[b]
1a	446	14530	540	94 (0.48)	0.68
1b	410	9220	553	143 (0.76)	0.42
2	435	25400	506	71 (0.40)	0.25

[a] Values in parentheses correspond to the energy difference in eV. [b] Fluorescence quantum yield (Φ_f) was determined relative to coumarin **6** as a standard (Φ_f = 0.78).[12]

Compound **1a** showed a red-shifted and more intense absorption spectrum compared to compound **1b** (Figure 2a), probably owing to its more planar structure, in turn due to its bulky hexyl chains pointing towards the less sterically hindered thiazole ring rather than the phenyl ring, as in the case of **1b**. The frontier orbital energy gaps estimated from the onset absorptions were in the 2.45–2.60 eV range, comparable to similar BBT derivatives.[39] Absorption spectra recorded at different concentrations presented the same shape (Figure S1, Supporting Information) which suggested the absence of dye aggregation, at least in the concentration range used in this work.

Both dyes displayed a brilliant green fluorescence in solution. They presented broad, featureless and fairly intense emission spectra in the 480 to 700 nm region (Figure 2a), which showed a mirror image relation with the corresponding absorption spectra and were relatively well-matched with the external quantum efficiency of the Si-based PV module used in the photovoltaic experiments (Figure S2). Interestingly, the spectrum of compound **1b** was the most red-shifted, with maximum at 553 nm compared to 540 nm for **1a**, thus giving a very large Stokes shift (SS) of 143 nm (compared to 94 nm for **1a**). Such observation could be explained considering the less planar structure of compound **1b**: after photoexcitation, the change induced in the electron density distribution could cause a more

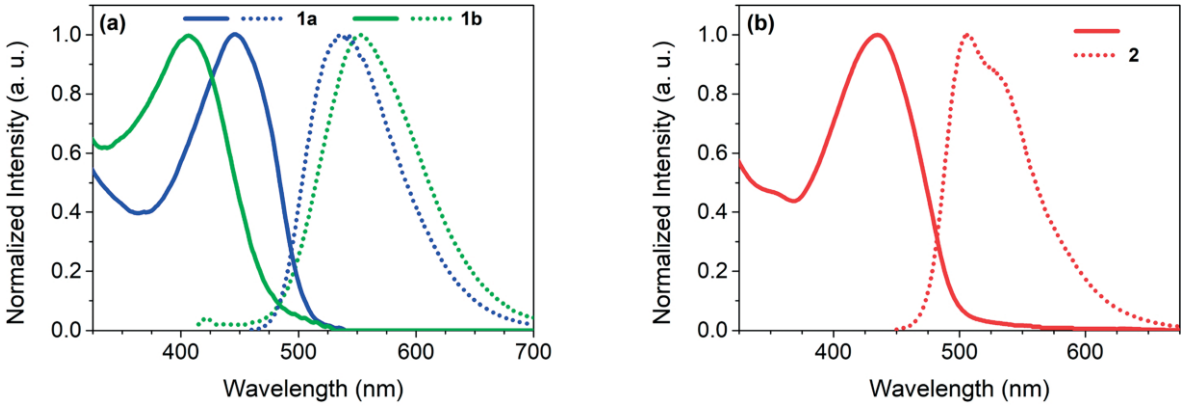

Figure 2. Normalized UV/Vis and fluorescence emission spectra in ethanol solution of: (a) compounds **1a** (blue line, conc. 1.0×10^{-5} M) and **1b** (green line, conc. 1.0×10^{-5} M); (b) compound **2** (red line, conc. 1.65×10^{-5} M).

pronounced nuclear motion during excited state geometry relaxation compared to the more planar and more conjugated structure of compound **1a**. Emission from this structurally relaxed excited state would explain the large values of Stokes shifts observed in this case. In agreement with the above explanation, fluorescence quantum yield (Φ_f) was higher for compound **1a**: this is not surprising, considering that with a decreasing energy difference between excited and ground state, the fluorescence intensity of fluorophores is known to decrease, owing precisely to enhanced vibrational relaxation and internal conversion.[40]

As anticipated, compound **2** presented relatively similar absorption and emission properties compared to fluorophores **1a** and **1b** (Figure 2b), but with some significant differences. Also in its case, the main absorption band was well-centered in the visible region with a maximum at 435 nm, while the molar extinction coefficient was larger than those of compounds **1a** and **1b**. Fluorescence emission for compound **2** was centered in the 480–640 nm region, and the corresponding band presented a maximum at 506 nm accompanied by a notable shoulder at lower energy. The latter feature was present also in the spectra recorded on more diluted solutions, and therefore it is more likely attributed to a vibronic structure rather than the formation of dimers/aggregates, as confirmed by the fact that the peak/shoulder ratio remained constant for all concentrations (Figure S1). Fluorescence quantum yield for **2** was estimated to be 0.25, thus much smaller than those obtained for BBT-derivatives.

In summary, for all the three fluorophores Stokes shifts appeared large enough to efficiently minimize re-absorption. In addition, fluorescence quantum yields, despite being lower than those of typical perylene-diimides,[9] were deemed compatible with the fabrication of test LSC devices.

Spectroscopic Characterization in PMMA Films

At this stage the opto-electronic properties of the new fluorophores were also investigated when dispersed in the transparent and totally amorphous matrix of PMMA. To evaluate the properties of BBT derivatives, **1a** was selected over **1b** because, on one hand, its red-shifted and more intense absorption spectrum guaranteed a superior solar light-harvesting ability and, on the other, it presented a clearly higher fluorescence quantum yield while retaining a sufficiently large Stokes shift.

The fluorophores were dispersed at different contents (0.2–1.4 wt.-%) in films of a thickness of 25 ± 5 μm with negligible phase-separation at the film surface for all the range of concentration investigated. In Figure 3a, the absorption characteristics of **1a**/PMMA films are reported. Compound **1a** in PMMA shows a molecular absorption maximum at about 450 nm with a broad absorption band at 370–510 nm, which results mostly similar to that recorded in ethanol solution. Notably, no evident absorption bands attributed to the formation of **1a** aggregates are observed, possibly due to the enhanced matrix compatibility provided by the *n*-hexyl groups linked to the thiophene rings. Indeed, absorbance intensities increase regularly and with a linear trend with **1a** content (Figure 3a, inset), that is without leveling off at the highest fluorophore content (i.e., 1.8 wt.-%).

Conversely, **1a**/PMMA films display emission features affected by fluorophore content (Figure 3b). When dispersed at low concentration in PMMA (i.e., 0.2 wt.-%), compound **1a** shows a fluorescence emission peaked at 540 nm with a Stokes shift of 90 nm, perfectly in agreement with results collected in solution. Compound **1a** is a strong emitter also in the solid phase when dispersed in PMMA with Φ_f slightly lower than that observed in solution (63 % against 68 %), despite the geometry constrains occurring in the glass matrix that prevent the dissipative phenomena potentially experienced in solution due to conformational changes.[41] Above this concentration, the fluorescence band significantly changed its look and emission quenching occurred although only to a certain extent (from 63 % to 45 % at the highest **1a** content). The emission shape variation with **1a** content might be possibly related to a combination of effects: first, increasing concentration in PMMA allows the emersion of the vibronic structure of **1a** emission; second, being the peak/shoulder ratio unrelated to concentration, fluorescence quenching of the monomeric form of **1a** can occur; third, the emersion of a red-shifted band at about 600 nm supports the formation of emissive **1a** aggregates within the PMMA matrix. Notably, the progressive red-shift of the fluorescence

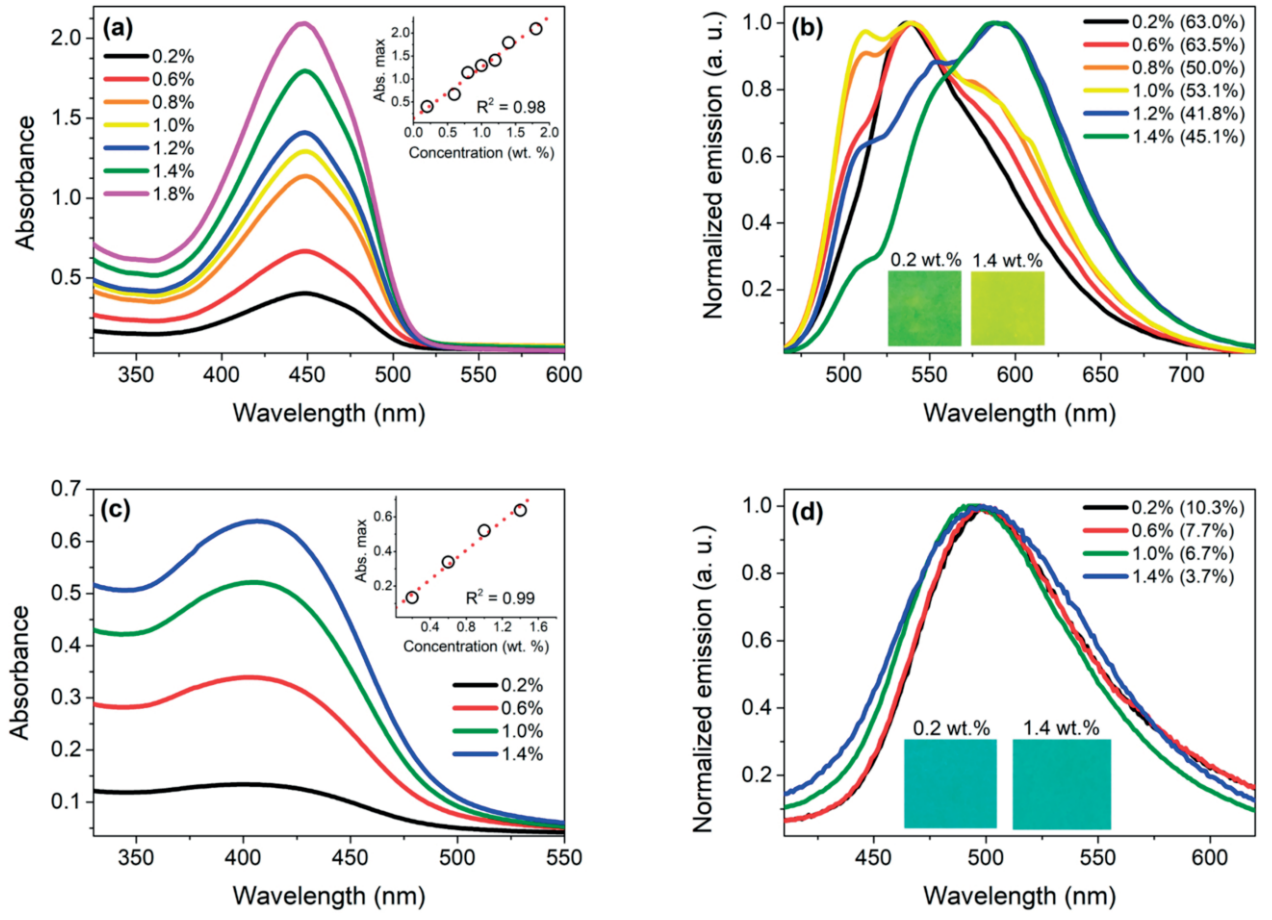

Figure 3. (a) UV/Vis absorption spectra of **1a**/PMMA films as a function of fluorophore concentration (wt.%). In the inset, the absorbance maximum at 450 nm was plotted as a function of **1a** content. (b) Fluorescence spectra of the same **1a**/PMMA films with excitation wavelength of 450 nm (absolute quantum yields are reported in parentheses). (c) UV/Vis absorption spectra of **2**/PMMA films as a function of fluorophore concentration (wt.%). In the inset, the absorbance maximum at 407 nm was plotted as a function of **2** content. (d) Fluorescence spectra of the same **2**/PMMA films with excitation wavelength of 390 nm (absolute quantum yields are reported in parentheses). In the inset of figures (b) and (d), pictures of the films taken under the excitation of a long-range UV lamp at 366 nm are shown.

band was also reflected on the color changes of the emission collected from **1a**/PMMA films excited by a long-range UV lamp at 366 nm (Figure 3b inset). Overall, thanks to all these phenomena occurring with concentration, fluorophore **1a** not only retained most of its fluorescence, but also acquired an emission spectrum better matching the external quantum efficiency of a typical Si-based PV module (Figure S2), thus making **1a**/PMMA films promising for the preparation of high efficiency LSCs at emission wavelengths near 600 nm.

In Figure 3c, the absorption features of **2**/PMMA films are reported. Compound **2** in PMMA shows a molecular absorption maximum at about 410 nm, that is 20 nm blue-shifted and with a broader and structure-less appearance with respect to that recorded in ethanol solution. Similar to what observed for **1a**/PMMA films, absorbance increased linearly with fluorophore content (Figure 3c, inset), that is without leveling off at the highest fluorophore concentration (i.e., 1.4 wt.-%).

Unlike compound **1a**, the emission of compound **2** was strongly and adversely affected in PMMA, even at the lowest fluorophore content (Figure 3d). Fluorescence, peaked at about 500 nm for all the PMMA films, was characterized by low Φ_f values, i.e. at least 2.5 times lower than that recorded in solution. Moreover, Φ_f dropped to about 4 % for PMMA film containing the highest content of dye **2**. This phenomenon could be interpreted on the basis of two distinct effects: the first is attributed to the broad absorption band of compound **2**, that could favor the occurrence of auto-absorption phenomena (i.e., inner-filter effects) and hence an overall poor emission intensity of the PMMA films already at the lowest dye concentration; the second involves the progressive formation of non-emissive aggregates of fluorophores increasing with the concentration of compound **2** in PMMA films.

Overall, **2**/PMMA films were characterized by a very weak emission and thus appeared much less suitable than those containing **1a** for applications in LSC/PV systems. Such hypothesis was confirmed by the subsequent photovoltaic measurements.

Optical Efficiency Determination of PMMA Films

The optical efficiencies (η_{opt}, see Exp. Sect. for the corresponding definition) of the LSC/PV systems based on fluorophores

1a and **2** were determined by coating optically pure 50 × 50 × 3 mm glass sheets with PMMA films featuring a thickness of 25 ± 5 μm. Photocurrent measurements were accomplished by illuminating the LSC with a solar simulator under AM1.5 conditions and by using a Si-based PV cell stuck onto one edge of the fluorescent collector (see Exp. Sect. for details). Values of η_{opt} are plotted in Figure 4 as a function of the different concentrations of fluorophores in the polymer matrix, and the best values are reported in Table 2.

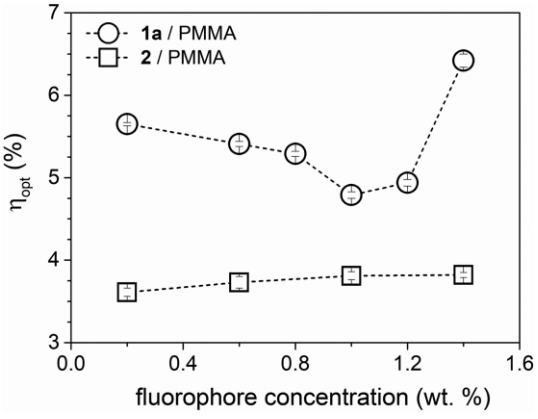

Figure 4. Optical efficiencies (η_{opt}) of **1a**/PMMA and **2**/PMMA films as a function of fluorophore concentration.

Table 2. Optical efficiencies (η_{opt}) determined for LSCs containing PMMA films of the different chromophores, and comparison with those of LR/PMMS LSCs with similar geometrical factor.

Entry	wt.%	η_{opt} [%]
1a/PMMA	0.2	5.65
	1.4	6.42
2/PMMA	1.4	3.82
LR/PMMA	1.5	7.21

Devices containing **1a**/PMMA films showed higher η_{opt} values than those determined for **2**/PMMA LSCs for all the range of concentrations investigated. This result is perfectly in line with the Φ_f values found earlier for the different PMMA films (Figure 3b and Figure 3d). Moreover, the ratio between Abs_{max} and fluorophore concentration calculated for **1a** in PMMA films was at least twice that of **2**/PMMA films (Figure 3a and Figure 3c, inset), thus indicating a superior capacity of **1a** to harvest light and, in turn to boost LSC performances. Being ε higher for compound **2** (Table 1), this behavior suggests a higher compatibility of **1a** in PMMA than **2**.[42,43] Notably, optical efficiency values for fluorophore **1a** were superior to 5.0 % at most concentrations, and reached the maximum value of 6.42 % for the 1.4 wt.-% sample, not far from those of state-of-the-art LSC devices containing perylene fluorophores in the same range of concentration [i.e. 7.21 % for 1.5 wt.-% of Lumogen Red (LR), Table 2].[23] The enhancement of η_{opt} value in passing from the 1.2 wt.-% to the 1.4 wt.-% sample could be explained considering the increased light collection due to the higher amount of dye in the film and the progressive red-shift of fluorophore emission, which counteracted re-absorption phenomena, causing a small increase of absolute quantum yield (Figure 3b). Films containing higher **1a** concentration showed lower values of optical efficiencies (e.g., 6.3 ± 0.1 % for the 1.8 wt.-% **1a**/PMMA film), thus indicating that fluorescence dissipation started to occur at that stage. On the other hand, **2**/PMMA LSCs exhibited nearly constant η_{opt} values around 3.6–3.8 % which were almost independent from the fluorophore content, probably because the increasing light collection according to the fluorophore concentration is counterbalanced by the progressive drop in Φ_f evidenced in the spectroscopic studies (Figure 3d).

Conclusions

In this work, we presented the synthesis and characterization of some organic fluorophore compounds containing either the benzo[1,2-*d*:4,5-*d*']bisthiazole (BBT) or the dithieno[3,2-*b*:2',3'-*d*]-silole (DTS) heterocyclic unit, in view of their employment for the fabrication of Luminescent solar concentrator (LSC) devices. Considering that one of the main objectives of LSC development is to reduce the cost of photovoltaic technology, compounds design was kept as simple as possible, in the hope to find an optimal compromise between facile and cheap synthetic procedures, reasonable optical properties and good efficiencies of the resulting PV devices.

All the synthesized compounds presented promising spectroscopic properties in solution, although benzobisthiazole derivatives **1a** and **1b** generally displayed larger Stokes shifts and higher fluorescence quantum yields compared to dithienosilole-based compound **2**. When dispersed in PMMA film at high concentration (1.2–1.4 wt.-%), fluorophore **1a** showed a red-shifted emission spectrum compared to solution, probably linked to the formation of red-emitting aggregates in the polymer matrix, but at the same time retained a good absolute quantum yield, which was deemed promising for its employment in LSC devices. In addition, such feature would allow to modulate the color of the film depending on the fluorophore content, which could be useful in view of the practical application of LSC devices in building-integrated photovoltaics (BIPV). Compound **2**, on the other hand, displayed decreasing Φ_f values with the increasing concentration, possibly due to re-absorption phenomena and the formation of non-emitting aggregates.

LSCs built with **1a**/PMMA films presented good optical efficiency values, reaching a maximum of 6.42 % for the 1.4 wt.-% sample. Even though optical efficiency values are hard to compare with those reported in the recent literature since they strongly depend on the LSC dimensions, the number of attached solar cells and the use of mirrors/scattering layer at the sides or backside, the best η_{opt} calculated for **1a**/PMMA films is promising and suggests that benzobisthiazole fluorophores could be a realistic alternative to perylene-based dyes in LSC/PV technology. Conversely, devices built with compound **2** provided clearly inferior results, indicating that, even in the presence of similar optical features in solution, the nature of the central heterocyclic core can have a tremendous impact on the photophysical properties of the corresponding compounds dispersed in PMMA and, in turn, on the photovoltaic performances of the resulting devices. Such observation highlights even

more the special suitability of the BBT heterocyclic unit towards insertion in the structure of LSC luminophores. The synthesis of novel heterocyclic compounds with improved spectroscopic properties and enhanced dispersability in polymer matrixes is currently ongoing and the corresponding investigations will be reported in due course.

Experimental Section

General Remarks

All commercially available compounds were purchased from *Merck KgaA*, *Fluorochem Ltd.* and *T.C.I. Co. Ltd.*, and were used without further purification unless stated otherwise. Anhydrous toluene and *N*,*N*-dimethylformamide (*N*,*N*-DMF) were obtained after drying with a *PureSolv Micro* apparatus (*Inert*). Dichloromethane was dried by distillation under nitrogen atmosphere and subsequent storage on activated molecular sieves (4 Å). Tetrahydrofuran was dried by distillation on metallic sodium using benzophenone as indicator, until the characteristic blue color of in situ-generated sodium diphenylketyl radical was found to persist. Diisopropylamine was distilled under inert atmosphere and kept over KOH. Organometallic reactions were carried out under dry nitrogen using Schlenk techniques. Solvent degassing was carried out according to the "freeze-pump-thaw" method. The temperature of –95 °C was obtained with a liquid N_2/acetone cooling bath. Reactions were monitored by TLC on Kieselgel 60 F254 (*Merck*) aluminum sheets and the products were visualized by exposing the plate to UV light or by staining it with $KMnO_4$ solution. Flash column chromatography[44] was performed using *Merck* Kieselgel 60 (300–400 mesh) as the stationary phase. ^{1}H-NMR spectra were recorded at 200–400 MHz, and ^{13}C-NMR spectra were recorded at 50.3–100.6 MHz, respectively, on *Varian* Gemini/Mercury/INOVA series instruments. Chemical shifts (δ) are reported in parts per million (ppm) and are referenced to the residual solvent peak ($CDCl_3$, δ = 7.26 ppm for ^{1}H-NMR and δ = 77.0 ppm for ^{13}C-NMR), while coupling constants (*J*) are reported in Hz. In some instances, 10 % v/v CF_3COOD (TFA-*d*) was added in the NMR tube to fully dissolve the analyzed compound [TFA-*d* gave the following signals in ^{13}C-NMR spectrum recorded in $CDCl_3$: δ = 161.7 (q, *J* = 43.3 Hz), 114.0 (q, *J* = 284.3 Hz)ppm]. GC/MS analyses of species with MW lower than 400 g/mol were performed using a *Shimadzu* QP505A gas-chromatograph. ESI-MS spectra were obtained by direct injection of the sample solution using a *Thermo Scientific* LCQ-FLEET instrument, while HRMS spectra were measured using a *Thermo Scientific* LTQ Orbitrap (FT-MS) instrument (carried out at the Interdepartmental Center for Mass Spectroscopy of the University of Florence, CISM); both are reported in the form *m*/*z*. UV/Vis spectra in solution were recorded with a *Varian Cary* 4000 spectrometer, and fluorescence spectra in solution were recorded with a *Varian Eclipse* instrument, irradiating the sample at the wavelength corresponding to maximum absorption in the UV spectrum.

Fluorescence quantum yields (Φ_f) in ethanol solution were determined at room temperature using coumarin **6** as the standard (Φ_f = 0.78 in EtOH)[12] using the following equation:[45]

$$\Phi_X = \Phi_{ST}\left(\frac{Grad_X}{Grad_{ST}}\right)\left(\frac{\eta_X^2}{\eta_{ST}^2}\right)$$

Where the subscripts X and ST indicate the sample and the standard, respectively, Grad is the gradient of the plot of integrated fluorescence intensity vs. absorbance for different solutions of the compounds and η is the refractive index of the corresponding solvents (EtOH for both solutions in the present case).

Poly(methyl methacrylate) (PMMA, Aldrich, M_w = 350 000 g mol^{-1}, acid number <1 mg KOH per g) and Lumogen Red F350 (LR, BASF) were used as received.

General Procedure for the Conversion of Thienyl Bromides in Aldehydes: In a Schlenk tube under an inert atmosphere of nitrogen, the appropriate thienyl bromide **3a**,**b** (1.0 equiv.) was dissolved in dry THF (1.5 mL per mmol of starting material). The resulting solution was cooled to –95 °C and *n*BuLi (1.6 M solution in hexanes, 1.05 equiv.) was added dropwise. The reaction mixture was stirred at –95 °C for 1 h, after which the reaction was quenched with anhydrous *N*,*N*-DMF (1.5 equiv.). The resulting mixture was slowly warmed up to room temp. while stirring overnight. A saturated aqueous solution of NH_4Cl (2 mL per mmol of starting material) was added, and the mixture was extracted with Et_2O (2 × 2.0 mL per mmol). The organic layer was washed with water (1.0 mL per mmol) and Brine (1.0 mL per mmol), and dried with Na_2SO_4. After removal of the solvent under reduced pressure, the residue was purified by flash column chromatography (SiO_2, CH_2Cl_2).

4a: Prepared starting from compound **3a** (1.24 g, 5.0 mmol). Purification by flash column chromatography afforded pure aldehyde **4a** as a dark yellow oil (814 mg, 4.1 mmol, 82 % yield). ^{1}H NMR (200 MHz, $CDCl_3$): δ = 10.03 (s, 1 H), 7.63 (d, *J* = 5.4 Hz, 1 H), 7.00 (d, *J* = 5.2 Hz, 1 H), 2.95 (t, *J* = 7.4 Hz, 2 H), 1.55–1.74 (m, 2 H), 1.21–1.40 (m, 6 H), 0.80–0.95 (m, 3 H) ppm. Spectroscopic data are in agreement with those reported in the literature.[46]

4b: Prepared starting from compound **3b** (1.24 g, 5.0 mmol). Purification by flash column chromatography afforded pure aldehyde **4b** as a brown oil (813 mg, 4.1 mmol, 82 % yield). ^{1}H NMR (200 MHz, $CDCl_3$): δ = 9.88 (d, *J* = 1.2 Hz, 1 H), 7.62 (d, *J* = 1.2 Hz, 1 H), 7.38 (s, 1 H), 2.65 (t, *J* = 7.6 Hz, 2 H), 1.60–1.68 (m, 2 H), 1.29–1.37 (m, 6 H), 0.86–0.93 (m, 3 H) ppm. Spectroscopic data are in agreement with those reported in the literature.[47]

General Procedure for the Formation of the Benzo[1,2-*d*:4,5-*d*′]-bisthiazole Ring: In a two necked round-bottom flask under an inert atmosphere of nitrogen, the appropriate aldehyde **4a**,**b** (1.0 equiv.) was dissolved in anhydrous toluene (2.5 mL per mmol of starting material). 2,5-Diaminobenzene-1,4-dithiol bis-hydrochloride (**5**, 0.25 equiv.) was then added, the reaction was heated to reflux and stirred for 16 h. After cooling to room temp., the mixture was diluted with CH_2Cl_2 (2.0 mL per mmol of starting material) and water (2.0 mL per mmol). The aqueous layer was washed with CH_2Cl_2 (2 × 3.0 mL per mmol). The combined organic layers were washed with water (3.0 mL per mmol) and Brine (3.0 mL per mmol), and dried with Na_2SO_4. After removal of the solvent under reduced pressure, the residue was purified by flash column chromatography (SiO_2, hexane/EtOAc, 20:1), followed by recrystallization from pentane.

6a: Prepared starting from compounds **4a** (550 mg, 3.02 mmol) and **5** (186 mg, 0.75 mmol). Purification by flash column chromatography/crystallization afforded pure benzobisthiazole **6a** as a yellow solid (181 mg, 0.35 mmol, 46 % yield). ^{1}H NMR (200 MHz, $CDCl_3$): δ = 8.49 (s, 2 H), 7.42 (d, *J* = 2.9 Hz, 2 H), 7.02 (d, *J* = 3.0 Hz, 2 H), 3.07 (t, *J* = 4.0 Hz, 4 H), 1.70–1.79 (m, 4 H), 1.21–1.43 (m, 12 H), 0.80–0.95 (m, 6 H) ppm. ^{13}C NMR (50 MHz, $CDCl_3$): δ = 161.5, 150.6, 144.9, 134.4, 131.4, 130.9, 128.4, 114.5, 31.6, 30.2, 30.1, 29.3, 22.6, 14.1 ppm. ESI-MS: *m*/*z* = 525.3 $[M + H]^+$.

6b: Prepared starting from compounds **4b** (550 mg, 3.02 mmol) and **5** (186 mg, 0.75 mmol). Purification by flash column chromatography/crystallization afforded pure benzobisthiazole **6b** as a yellow solid (200 mg, 0.38 mmol, 51 % yield). ^{1}H NMR (400 MHz, $CDCl_3$): δ = 8.40 (s, 2 H), 7.52 (d, *J* = 1.2 Hz, 2 H), 7.13 (d, *J* = 1.2 Hz, 2 H),

2.65 (t, J = 7.7 Hz, 4 H), 1.62–1.72 (m, 4 H), 1.27–1.48 (m, 12 H), 0.82–0.96 (m, 6 H) ppm. Spectroscopic data are in agreement with those reported in the literature.[27]

General Procedure for the Electrophilic Bromination of BBT Derivatives: In a round-bottom flask under an inert atmosphere of nitrogen, the appropriate benzobisthiazole **6a**,**b** (1.0 equiv.) was dissolved in a 1:1 mixture (v/v) of $CHCl_3$ and glacial acetic acid (25 mL per mmol of starting material). *N*-bromosuccinimide (NBS, 2.5 equiv.) was then added, the flask was shielded from light using aluminum foil and the reaction mixture was stirred at room temp. for 16 h. After this time, the reaction was quenched by addition of water (15 mL per mmol of starting material). The aqueous layer was extracted with CH_2Cl_2 (2 × 15 mL per mmol), and the combined organic layers were washed with water (20 mL per mmol) and brine (20 mL per mmol), and dried with Na_2SO_4. After removal of the solvent under reduced pressure, the residue was purified by flash column chromatography (SiO_2, petroleum ether/EtOAc, 50:1), if necessary followed by recrystallization from pentane.

7a: Prepared starting from compound **6a** (184 mg, 0.35 mmol) and NBS (157 mg, 0.88 mmol). Purification by flash column chromatography/crystallization afforded pure dibromide **7a** as a yellow solid (126 mg, 0.19 mmol, 53 % yield). ^{1}H NMR (400 MHz, $CDCl_3$ + 10 % v/v TFA-*d*): δ = 8.81 (s, 2 H), 7.28 (s, 2 H), 3.00 (t, J = 7.9 Hz, 4 H), 1.75–1.85 (m, 4 H), 1.44–1.54 (m, 4 H), 1.30–1.39 (m, 8 H), 0.91 (t, J = 6.9 Hz, 6 H) ppm. ^{13}C NMR (100 MHz, $CDCl_3$ + 10 % v/v TFA-*d*): δ = 165.8, 155.6, 140.1, 135.7, 131.7, 127.4, 124.7, 112.6, 31.4, 31.2, 29.4, 29.1, 22.4, 13.8 ppm. ESI-MS: m/z = 685.3, 683.2, 681.2 (1:2:1) $[M + H]^+$.

7b: Prepared starting from compound **6b** (184 mg, 0.35 mmol) and NBS (157 mg, 0.88 mmol). Purification by flash column chromatography afforded pure dibromide **7b** as a yellow solid (105 mg, 0.15 mmol, 44 % yield). ^{1}H NMR (400 MHz, $CDCl_3$): δ = 8.39 (s, 2 H), 7.36 (s, 2 H), 2.60 (t, J = 7.6 Hz, 4 H), 1.27–1.40 (m, 16 H), 0.86–0.96 (m, 6 H) ppm. Spectroscopic data are in agreement with those reported in the literature.[28]

General Procedure for the Double Suzuki–Miyaura Coupling of BBT Derivatives: In a MW vial under an inert atmosphere of nitrogen, the appropriate dibromide **7a**,**b** (1.0 equiv.) was dissolved in degassed toluene (55 mL per mmol of starting material). In a separate Schlenk flask under an inert atmosphere of nitrogen was prepared a solution of KF (6.0 equiv.), $[Pd(dppf)Cl_2]$ (0.05 equiv.) and boronic acid **8** (4.0 equiv.) in MeOH (10 mL per mmol of starting material). After complete dissolution, the latter mixture was added in the MW vial and the resulting solution was stirred at room temp. for 30′. The vial was then placed in the MW reactor and the reaction mixture was heated at 70 °C for 35′. After removal of the solvent under reduced pressure, the residue was purified by flash column chromatography (SiO_2, petroleum ether/toluene/CH_2Cl_2, 3:1:2), followed by crystallization from *n*-hexane.

1a: Prepared from dibromide **7a** (40 mg, 0.06 mmol), compound **8** (68 mg, 0.24 mmol, 4.0 equiv.), $[Pd(dppf)Cl_2]$ (2.2 mg, 3 μmol, 0.05 equiv.) and KF (21 mg, 0.36 mmol, 6.0 equiv.). Purification by flash column chromatography/crystallization afforded compound **1a** as an orange solid (23 mg, 0.022 mmol, 38 % yield). ^{1}H NMR (400 MHz, $CDCl_3$): δ = 8.43 (s, 2 H), 7.53 (d, J = 8.8 Hz, 4 H), 7.26–7.32 (m, 8 H), 7.11–7.17 (m, 10 H), 7.06–7.11 (m, 8 H), 3.03 (t, J = 7.9 Hz, 4 H), 1.73–1.83 (m, 4 H), 1.46–1.55 (m, 4 H), 1.32–1.41 (m, 8 H), 0.88–0.95 (m, 6 H) ppm. ^{13}C NMR (100 MHz, $CDCl_3$): δ = 161.0, 150.5, 148.1, 147.2, 146.5, 145.9, 134.4, 129.7, 129.4, 127.1, 126.6, 125.8, 124.8, 123.4, 123.0, 114.1, 31.7, 30.4, 30.1, 29.4, 22.6, 14.1 ppm. ESI-MS: m/z = 1011.6 $[M + H]^+$. HRMS (ESI) for $C_{64}H_{59}N_4S_4$ $[M + H]^+$: calcd. 1011.3617, found 1011.3604.

1b: Prepared from dibromide **7b** (40 mg, 0.06 mmol), compound **8** (68 mg, 0.24 mmol, 4.0 equiv.), $[Pd(dppf)Cl_2]$ (2.2 mg, 3 μmol, 0.05 equiv.) and KF (21 mg, 0.36 mmol, 6.0 equiv.). Purification by flash column chromatography/crystallization afforded compound **1b** as an orange solid (18 mg, 0.018 mmol, 30 % yield). ^{1}H NMR (400 MHz, $CDCl_3$): δ = 8.41 (s, 2 H), 7.56 (s, 2 H), 7.33–7.38 (m, 4 H), 7.27–7.33 (m, 8 H), 7.14–7.19 (m, 8 H), 7.05–7.14 (m, 8 H), 2.71 (t, J = 7.8 Hz, 4 H), 1.63–1.73 (m, 4 H), 1.27–1.40 (m, 12 H), 0.86–0.92 (m, 6 H) ppm. ^{13}C NMR (100 MHz, $CDCl_3$): δ = 162.2, 151.7, 147.8, 147.3, 142.9, 139.5, 134.1, 133.8, 131.6, 129.8, 129.4, 127.0, 124.9, 123.4, 122.5, 114.6, 31.6, 30.9, 29.7, 29.2, 22.6, 14.1 ppm. ESI-MS: m/z = 1011.2 $[M + H]^+$. HRMS (ESI) for $C_{64}H_{59}N_4S_4$ $[M + H]^+$: calcd. 1011.3617, found 1011.3613.

11: In a round-bottom flask under an inert atmosphere of nitrogen, compound **10**[38] (260 mg, 0.61 mmol,1.0 equiv.) was dissolved in CH_2Cl_2 (5 mL). *N*-bromosuccinimide (NBS, 274 mg, 1.54 mmol, 2.5 equiv.) was then added, the flask was shielded from light using aluminum foil and the reaction mixture was stirred at room temp. for 3 h. After this time, the reaction was quenched by addition of water (10 mL). The aqueous layer was extracted with CH_2Cl_2 (2 × 10 mL), and the combined organic layers were washed with water (20 mL) and brine (20 mL), and dried with Na_2SO_4. After removal of the solvent under reduced pressure, the residue was purified by flash column chromatography (SiO_2, petroleum ether) to yield compound **11** as a yellow oil (330 mg, 0.58 mmol, 95 % yield). ^{1}H NMR (200 MHz, $CDCl_3$): δ = 6.99 (s, 2 H), 1.05–1.45 (m, 24 H), 0.75–0.95 (m, 10 H) ppm. The spectroscopic data are in agreement with those reported in the literature.[48]

2: In a Schlenk tube under an inert atmosphere of nitrogen were placed dibromide **11** (47 mg, 0.082 mmol, 1.0 equiv.), 4-(diphenylamino)benzene boronic acid (**8**, 71 mg, 0.25 mmol, 3.0 equiv.), $Pd(OAc)_2$ (1.0 mg, 4.1 μmol; 0.05 equiv.), P(o-tolyl)$_3$ (2.5 mg, 8.2 μmol, 0.1 equiv.) and K_2CO_3 (2.0 M, 0.12 mL), dissolved in degassed toluene (3.0 mL). The solution was further degassed for 10 min, it was heated at 75 °C and then stirred for 3 d. After cooling to room temp., water (5 mL) was added to the reaction mixture, and the aqueous layer was extracted with CH_2Cl_2 (3 × 5 mL). The combined organic layers were washed with water (10 mL) and brine (10 mL), and dried with Na_2SO_4. After removal of the solvent under reduced pressure, the residue was purified by flash column chromatography (SiO_2, starting with petroleum ether then petroleum ether/CH_2Cl_2, 20:1 then petroleum ether/CH_2Cl_2, 10:1) to give compound **2** as a yellow solid (46 mg, 0.051 mmol, 62 % yield). ^{1}H NMR (400 MHz, $CDCl_3$): δ = 7.22–7.50 (m, 12 H), 7.00–7.20 (m, 18 H), 1.37–1.45 (m, 4 H), 1.15–1.35 (m, 20 H), 0.90–0.98 (m, 4 H), 0.85 (t, J = 7.0 Hz, 6 H) ppm. ^{13}C NMR (100.6 MHz, $CDCl_3$): δ = 147.8, 147.6, 146.8, 144.9, 134.8, 129.2, 127.3, 126.4, 124.4, 124.3, 124.1, 122.8, 33.2, 31.9, 29.7, 29.2, 24.2, 22.7, 14.1, 12.0 ppm. ESI-MS: m/z = 904.8 $[M]^+$. HRMS (ESI) for $C_{60}H_{64}N_2S_2Si$ $[M]^+$: calcd. 904.4275, found 904.4284.

Preparation of 1a/PMMA and 2/PMMA Polymer Films: 1a/PMMA and **2**/PMMA films were prepared with fluorophore to polymer concentrations of 0.1–1.8 wt.-%. The fluorophores were dissolved in chloroform in a ratio of 1.2 mg/mL by stirring continuously for 30 min at ambient temperature. Specific volumes of these mixtures were added to 60 mg PMMA and supplemented with extra chloroform so that concentrations in the range of 0.1–1.8 wt.-% fluorophore to PMMA in 1.4 mL chloroform were obtained. Subsequently, the mixtures were spread out evenly on thoroughly cleaned glass plates (50 × 50 × 3 mm). The product was obtained after evaporation at room temperature in a closed environment.

Spectroscopic Characterization of Films: Spectrophotometric measurements were performed using a Perkin–Elmer Lambda 650 spectrometer. Fluorescence spectra in the solid state were measured at room temperature by a Horiba Jobin–Yvon Fluorolog®-3 spectrofluorometer equipped with a 450 W Xenon arc lamp and double-grating both excitation and emission monochromators. The emission quantum yields of the solid samples were obtained by means of a 152 mm diameter "Quanta-φ" integrating sphere, coated with Spectralon®, using as excitation source the 450 W Xenon lamp coupled with a double-grating monochromator for selecting wavelengths. The Quanta-φ apparatus was coupled to the spectrofluorometer by a 1.5 m fiber-optic bundle in a slit-round configuration, 180 fibers; slit-end termination 10 mm O.D. × 50 mm long; round-end termination FR-274; the sheath is PVC monocoil.

Optical Efficiency Measurements: A home-built equipment setup was utilized to measure the efficiency of the LSCs. Each fluorophore concentration was tested in triplicate. A sample holder with the photovoltaic (PV) module (IXYS SLMD121H08L mono solar cell 86 × 14 mm: V_{oc} = 5.04 V, I_{sc} = 50.0 mA, FF > 70 %, η_{PV} = 22 %) is placed 2.5 cm above a scattering layer. The PV cell is masked with black tape to match LSC edge (50 × 3 mm) so that limiting the stray light to negligible levels. Silicon was used to grease the LSC edge. The other three edges of the LSC were covered with a reflective aluminum tape. A solar simulating lamp (ORIEL® LCS-100 solar simulator 94011A S/N: 322, AM1.5G std filter: 69 mW/cm^{-2} at 254 mm) was housed 27.5 cm above the sample. The PV module was connected to a digital potentiometer (AD5242) controlled via I2C by an Arduino Uno (https://www.arduino.cc) microcontroller using I2C master library. A digital multimeter (KEITHLEY 2010) was connected in series with the circuit, between the PV module and the potentiometer, to collect the current as a function of the external load. Conversely, the voltage was measured by connecting the multimeter in parallel to the digital potentiometer. Arduino Uno controlled the multimeter via SCPI language over RS-232 bus using a TTL to RS-232 converter chip (MAX232). Arduino Uno was connected to pc via USB port and controlled by a Python script. The measurement cycle began with a signal from PC to Arduino which set the multimeter parameter to measure current. Then, Arduino began the measure loop: (1) set the potentiometer to a given value; (2) send a trigger signal to the multimeter; (3) read the measured data and (4) send the data back to PC. The loop is repeated 256 times for potentiometer values ranging 60 Ω to 1 MΩ. Arduino set the multimeter to measure voltage and for each potentiometer value the system recorded 8 data samples which were subsequently processed by the Python script. A schematic representation of the apparatuses used for photocurrent and photovoltage measurements is reported in Figure S3-S4. The optical efficiency was reported as η_{opt} and obtained from the concentration factor (*C*), which is the ratio between the maximal current of the PV cell attached the LSC edges under illumination of a light source and the maximal current of the bare cell put perpendicular to the light source.[25]

Formulas for Efficiency Calculations

$$C = \frac{I_{LSC}}{I_{SC}}$$

$$\eta_{opt} = \frac{I_{LSC}}{G \cdot I_{SC}}$$

where *C* is the concentration factor, η_{opt} is the optical efficiency, I_{LSC} is the short-circuit current measured for the cell placed on the edge of the luminescent solar concentrator, I_{SC} is the short-circuit current measured for the bare cell placed perpendicularly to the light source and G is the device geometrical factor, corresponding to the surface area ratio (A_{LSC}/A_{SC} = 16.6 in our setup).

Acknowledgments

The authors are grateful to the "Cassa di Risparmio di Firenze" foundation ("ENERGYLAB" project) for financial support. In addition, Mr. Quentin Lemoine is acknowledged for his collaboration in the preparation of compound **2** and Mr. Giuseppe Iasilli for his assistance in the determination of the LSC performances.

Keywords: Functional organic materials · Organic fluorophores · Luminescence · Solar cells · Photovoltaics

[1] V. Balzani, N. Armaroli, *Energy for a Sustainable World*, Wiley-VCH, Weinheim, **2010**.
[2] *PV Status Report **2017***, Joint Research Centre of the European Commission, November 2017.
[3] *Current and Future Cost of Photovoltaics. Long-term Scenarios for Market Development, System Prices and LCOE of Utility-Scale PV Systems. Study on behalf of Agora Energiewende.* Fraunhofer ISE, February **2015**.
[4] M. Wiesenfarth, S. P. Philipps, A. W. Bett, K. Horowitz, S. Kurtz, *Current Status of Concentrator Photovoltaic (CPV) Technology (v1.3)*, Fraunhofer ISE/NREL, April **2017**.
[5] W. G. J. H. M. van Sark, *Renewable Energy* **2013**, *49*, 207–210.
[6] M. Debije, *Nature* **2015**, *519*, 298–299.
[7] M. G. Debije, P. P. C. Verbunt, *Adv. Energy Mater.* **2012**, *2*, 12–35.
[8] A. Goetzberger, W. Greube, *Appl. Phys.* **1977**, *14*, 123–139.
[9] L. Beverina, A. Sanguineti in *Solar Cell Nanotechnology* (Eds.: A. Tiwari, R. Boukherroub, M. Sharon), Scrivener Publishing LLC, Beverly, **2014**, pp. 317–356.
[10] Y. Zhou, D. Benetti, Z. Fan, H. Zhao, D. Ma, A. O. Govorov, A. Vomiero, F. Rosei, *Adv. Energy Mater.* **2016**, *6*, 1501913.
[11] M. Carlotti, G. Ruggeri, F. Bellina, A. Pucci, *J. Lumin.* **2016**, *171*, 215–220.
[12] B. Valeur, M. N. Berberan-Santos, *Molecular Fluorescence: Principles and Applications*, Wiley-VCH, Weinheim, **2013**.
[13] B. McKenna, R. C. Evans, *Adv. Mater.* **2017**, *29*, 1606491.
[14] A. Sanguineti, M. Sassi, R. Turrisi, R. Ruffo, G. Vaccaro, F. Meinardi, L. Beverina, *Chem. Commun.* **2013**, *49*, 1618–1620.
[15] W. E. Benjamin, D. R. Veit, M. J. Perkins, E. Bain, K. Scharnhorst, S. McDowall, D. L. Patrick, J. D. Gilbertson, *Chem. Mater.* **2014**, *26*, 1291–1293.
[16] J. ter Schiphorst, A. M. Kendhale, M. G. Debije, C. Menelaou, L. M. Herz, A. P. H. J. Schenning, *Chem. Mater.* **2014**, *26*, 3876–3878.
[17] R. Turrisi, A. Sanguineti, M. Sassi, B. Savoie, A. Takai, G. E. Patriarca, M. M. Salamone, R. Ruffo, G. Vaccaro, F. Meinardi, T. J. Marks, A. Facchetti, L. Beverina, *J. Mater. Chem. A* **2015**, *3*, 8045–8054.
[18] Application of the "latent pigment approach" to PDMI flurophores: S. Mattiello, A. Sanzone, P. Brazzo, M. Sassi, L. Beverina, *Eur. J. Org. Chem.* **2015**, 5723–5729.
[19] A. Kaniyoor, B. McKenna, S. Comby, R. C. Evans, *Adv. Opt. Mater.* **2016**, *4*, 444–456.
[20] a) W. Zhou, M.-C. Wang, X. Zhao, *Sol. Energy* **2015**, *115*, 569–576; b) W. Zhou, M.-C. Wang, X. Zhao, *Sol. Energy* **2015**, *120*, 419–427.
[21] F. Bellina, C. Manzini, G. Marianetti, C. Pezzetta, E. Fanizza, M. Lessi, P. Minei, V. Barone, A. Pucci, *Dyes Pigm.* **2016**, *134*, 118–128.
[22] a) C. Botta, P. Betti, M. Pasini, *J. Mater. Chem. A* **2013**, *1*, 510–514; b) A. Iagatti, B. Patrizi, A. Basagni, A. Marcelli, A. Alessi, S. Zanardi, R. Fusco, M. Salvalaggio, L. Bussotti, P. Foggi, *Phys. Chem. Chem. Phys.* **2017**, *19*, 13604–13613.
[23] J. Lucarelli, M. Lessi, C. Manzini, P. Minei, F. Bellina, A. Pucci, *Dyes Pigm.* **2016**, *135*, 154–162.
[24] F. De Nisi, R. Francischello, A. Battisti, A. Panniello, E. Fanizza, M. Striccoli, X. Gu, N. L. C. Leung, B. Z. Tang, A. Pucci, *Mater. Chem. Front.* **2017**, *1*, 1406–1412.
[25] F. Gianfaldoni, F. De Nisi, G. Iasilli, A. Panniello, E. Fanizza, M. Striccoli, D. Ryuse, M. Shimizu, T. Biver, A. Pucci, *RSC Adv.* **2017**, *7*, 37302–37309.

[26] N. J. L. K. Davis, R. W. MacQueen, S. T. E. Jones, C. Orofino-Pena, D. Cortizo-Lacalle, R. G. D. Taylor, D. Credgington, P. J. Skabara, N. C. Greenham, *J. Mater. Chem. C* **2017**, *5*, 1952–1962.
[27] R. Rondão, A. R. Frias, S. F. H. Correia, L. Fu, V. de Zea Bermudez, P. S. André, R. A. S. Ferreira, L. D. Carlos, *ACS Appl. Mater. Interfaces* **2017**, *9*, 12540–12546.
[28] A. Dessì, G. Barozzino Consiglio, M. Calamante, G. Reginato, A. Mordini, M. Peruzzini, M. Taddei, A. Sinicropi, M. L. Parisi, F. Fabrizi de Biani, R. Basosi, R. Mori, M. Spatola, M. Bruzzi, L. Zani, *Eur. J. Org. Chem.* **2013**, 1916–1928.
[29] T. Sasaki, T. Inoue, Y. Komori, S. Irie, K. Sakurai, K. Tsubakiyama, *Phys. Chem. Chem. Phys.* **2003**, *5*, 1381–1385.
[30] See, for example: M. M. Alam, S. A. Jenekhe, *Chem. Mater.* **2002**, *14*, 4775–4780 and references cited therein.
[31] S. Yao, H.-Y. Ahn, X. Wang, J. Fu, E. W. Van Stryland, D. J. Hagan, K. D. Belfield, *J. Org. Chem.* **2010**, *75*, 3965–3974.
[32] M. Zhang, X. Guo, Y. Li, *Adv. Energy Mater.* **2011**, *1*, 557–560.
[33] H. Fu, Y. Chen, *Curr. Org. Chem.* **2012**, *16*, 1423–1446.
[34] a) T. Lee, I. Jung, K. H. Song, H. Lee, J. Choi, K. Lee, B. J. Lee, J. Pak, C. Lee, S. O. Kang, J. Ko, *Organometallics* **2004**, *23*, 5280–5285; b) J. Ohshita, Y. Kurushima, K.-H. Lee, A. Kunai, Y. Ooyama, Y. Harima, *Organometallics* **2007**, *26*, 6591–6595; c) H. Jung, H. Hwang, K.-M. Park, J. Kim, D.-H. Kim, Y. Kang, *Organometallics* **2010**, *29*, 2715–2723; d) H. Park, Y. Rao, M. Varlan, J. Kim, S.-B. Ko, S. Wang, Y. Kang, *Tetrahedron* **2012**, *68*, 9278–9283; e) J. Ohshita, Y. Tominaga, D. Tanaka, Y. Ooyama, T. Mizumo, N. Kobayashi, H. Higashimura, *Dalton Trans.* **2013**, *42*, 3646–3652.
[35] C. Zhang, C. Sun, Y. Lu, J. Wang, X. He, J. Lu, S. Yin, H. Qiu, *Spectrochim. Acta Part A* **2015**, *150*, 731–736.
[36] E. H. Elandaloussi, P. Frère, P. Richomme, J. Orduna, J. Garin, J. Roncali, *J. Am. Chem. Soc.* **1997**, *119*, 10774–10784.
[37] Lower yields of the product (in the 10–30 % range) were obtained when using other typical palladium catalysts, such as $Pd(PPh_3)_4$, as well as alkaline carbonate bases.
[38] P. M. Beaujuge, H. N. Tsao, M. R. Hansen, C. M. Amb, C. Risko, J. Subbiah, K. R. Choudhury, A. Mavrinskiy, W. Pisula, J.-L. Bredas, F. So, K. Müllen, J. R. Reynolds, *J. Am. Chem. Soc.* **2012**, *134*, 8944–8957.
[39] M. Mamada, J.-i. Nishida, S. Tokito, Y. Yamashita, *Chem. Lett.* **2008**, *37*, 766–767.
[40] M. Sauer, J. Hofkens, J. Enderlein, *Handbook of Fluorescence Spectroscopy and Imaging*, Wiley-VCH, Weinheim, **2011**, pp. 1–30.
[41] G. Del Frate, F. Bellina, G. Mancini, G. Marianetti, P. Minei, A. Pucci, V. Barone, *Phys. Chem. Chem. Phys.* **2016**, *18*, 9724–9733.
[42] F. Ciardelli, G. Ruggeri, A. Pucci, *Chem. Soc. Rev.* **2013**, *42*, 857–870.
[43] A. Pucci, N. Tirelli, G. Ruggeri, F. Ciardelli, *Macromol. Chem. Phys.* **2005**, *206*, 102–111.
[44] W. C. Still, M. Kahn, A. Mitra, *J. Org. Chem.* **1978**, *43*, 2923–2925.
[45] A. M. Brouwer, *Pure Appl. Chem.* **2011**, *83*, 2213–2228.
[46] S. Barriga, P. Fuertes, C. F. Marcos, O. A. Rakitin, T. Torroba, *J. Org. Chem.* **2002**, *67*, 6439–6448.
[47] I. H. Jung, Y. K. Jung, J. Lee, J.-H. Park, H. Y. Woo, J.-I. Lee, H. Y. Chu, H.-K. Shim, *J. Polym. Sci., Part A: Polym. Chem.* **2008**, *46*, 7148.
[48] R. Grisorio, G. P. Suranna, P. Mastrorilli, G. Allegretta, A. Loiudice, A. Rizzo, G. Gigli, K. Manoli, M. Magliulo, L. Torsi, *J. Polym. Sci., Part A: Polym. Chem.* **2013**, *51*, 4860–4872.

Received: February 12, 2018